

Probing the “Sea” of Galactic Cosmic Rays with *Fermi*-LAT

Felix Aharonian*

Dublin Institute for Advanced Studies, 31 Fitzwilliam Place, Dublin 2, Ireland
Max-Planck-Institut für Kernphysik, P.O. Box 103980, 69029 Heidelberg, Germany

Giada Peron,[†] Ruizhi Yang,[‡] and Roberta Zanin[§]

Max-Planck-Institut für Kernphysik,
P.O. Box 103980, 69029 Heidelberg, Germany

Sabrina Casanova[¶]

Max-Planck-Institut für Kernphysik, P.O. Box 103980, 69029 Heidelberg, Germany
Institute of Nuclear Physics, Radzikowskiego 152, 31-342 Krakow, Poland

(Dated: Received: / Accepted:)

High energy γ rays from Giant Molecular Clouds (GMCs) carry direct information about spatial and energy distributions of Galactic Cosmic Rays (CRs). The recently released catalogues of GMCs contain sufficiently massive clouds to be used as barometers for probing, through their γ -ray emission, the density of CRs throughout the Galactic Disk. Based on the data of *Fermi*-LAT, we report the discovery of γ -ray signals from fifteen GMCs located at distances from 0.6 kpc to 12.5 kpc. The Galactocentric radial distribution of the CR density derived from the γ -ray and CO observations of these objects, as well as from some nearby clouds belong the Gould Belt complex, unveil a homogeneous “sea” of CRs with a constant density and spectral shape close to the flux of directly (locally) measured CRs. The only exception we found in some locations characterized by enhanced CR density in the 4-6 kpc ring. We argue that the latter is not related to a global variation of the CR sea but has a local character caused by the presence of CR accelerators in the densely populated star-forming regions within the 4-6 kpc ring.

PACS numbers: 95.85.Ry; 98.70.Sa

The recent several years have been marked by impressive progress in the precision and quality of Cosmic Ray (CR) measurements, including the detection of a substantial hardening of the energy spectrum of protons and nuclei above 100 GeV/amu [1, 2]), the extension of the electron spectrum, after the break around 1 TeV [3], to energy of 20 TeV [4], the discovery of anomalously high content of secondary positrons and antiprotons [5], *etc.* The new measurements represent an added value to our knowledge about CRs. Yet, the key issues concerning the origin of Galactic CRs are not fully understood and resolved.

A breakthrough in the field is expected from γ -ray observations. This concerns both the acceleration and propagation aspects of CR studies. While the detection and identification of γ -ray sources unveil the sites of CR production, the diffuse γ -ray emission of the Galactic Disk contains information about the spatial and energy distributions of CRs. The accumulation and effective mixture of relativistic particles through their convection and diffusion in the interstellar magnetic fields results in the formation of the so-called *sea* of Galactic CRs. The level and the energy spectrum of the CR sea is determined by the operation of all galactic accelerators over the confinement time of CRs which can be determined directly from CR measurements, namely, from the secondary-to-primary ratio. At low (GeV) energies it is estimated

about 10^7 yrs, and decreases with energy as $E^{-\delta}$, with $\delta \sim 0.3 - 0.5$. The latter reflects the energy dependence of the diffusion coefficient. Since the effective “lifetime” of suspected CRs accelerators is shorter than the confinement time, one expects rather homogeneous distribution of CRs on large (kpc) scales. The homogeneity of CRs, however, can be violated on smaller scales, in the form of *excess* fluxes over the CR sea, caused by the injection of freshly accelerated particles into the ISM.

The diffuse galactic γ radiation produced over six decades in energy at interactions of relativistic electrons, protons and nuclei with the interstellar medium (ISM) and radiation fields, is contributed by different radiation mechanisms. Remarkably, the energy interval from 100 MeV to 100 GeV is undoubtedly dominated by γ -rays from the decays of π^0 mesons produced at interactions of CRs with the interstellar gas [6, 7]. This allows us to measure the *mean* density of Galactic CRs in different directions averaged along the line of sight, since $\rho_{\text{CR}} \propto F_{\gamma}/n_{\text{H}}$, where F_{γ} and n_{H} are the γ -rays flux and the gas column density in the given direction of ISM, respectively.

Gamma rays from *individual* Giant Molecular Clouds (GMCs) provide more straightforward (localized) information about the CR density, thus serving as unique CR barometers distributed throughout the Galaxy [8, 9]. The case of *passive* GMCs, i.e. clouds located far from active accelerators where the CR density is dominated

by the CR sea, is of special interest. The detection of γ rays from such clouds tells us about the level of the CR sea without substantial contamination by particles injected by nearby objects. The flux of γ -rays from “passive” clouds depends linearly only on the parameter, $A \equiv M_5/d_{\text{kpc}}^2$, where $M_5 = M/10^5 M_\odot$ and $d_{\text{kpc}} = d/1$ kpc. Typically, γ -rays from passive clouds can be detected by *Fermi*-LAT when $A \sim 1$. In the case of location of compact clouds in uncrowded regions, the detection threshold can be reduced down to 0.2. On the other hand, for very close clouds, $d \ll 1$ kpc, A should significantly exceed 1 to compensate the loss of the sensitivity of *Fermi*-LAT due to the large (several degree) angular extensions of clouds.

In the case of Sgr B2, located in the Galactic Center (GC), the reduction of the flux due to the large distance of $d \simeq 8.5$ kpc, is compensated by the huge mass of $M \sim 10^7 M_\odot$ and the small angular extension of ~ 10 arcmin. The reported results show that in these two essentially different parts of the Galaxy the CR fluxes do not deviate from the local (directly measured) CR flux. Could we interpret this as a hint of detection of the CR sea? Apparently, such a statement must be supported by a larger number of γ -ray emitting clouds broadly distributed over the Galactic Plane. Until recently, because of the lack of information about the presence of adequately massive clouds, the realization of this task with *Fermi*-LAT could seem unrealistic. However, recently, a catalog of Galactic GMCs containing clouds of unexpectedly large masses has been released [10] which makes them as potentially detectable targets by *Fermi*-LAT from very large distances, up to 12 kpc from us.

The catalog consists of 1064 objects. These objects are distributed in the Galactic Disk between $180^\circ > l > 13^\circ$ and $348^\circ > l > 180^\circ$ within $-5^\circ < b < 5^\circ$ and are widely spread in the Galaxy covering distances from the GC from ~ 2 to ~ 15 kpc. Approximately 4% of these clouds have masses between 10^6 and $10^7 M_\odot$. In this work we report the results of analysis of 12 clouds from this catalog. The selection has been performed based on the following criteria. First, we have selected clouds expected to be bright in γ -rays, i.e. the clouds with large values of the A parameter. Given the average *Fermi*-LAT flux sensitivity for extended sources in the Galactic Plane, we set a threshold, $A > 0.4$. In this way, 34 clouds have been selected from the list presented in ref.[10]. In the second stage, we required that the chosen cloud dominates the gas column density in the given direction. We considered the brightness temperature vs. velocity profile of CO (extracted from ref.[11]) as a tracer of H_2 , and of HI (from ref. [12]) and calculated the relative contribution in the region of the cloud (see Table III in the supplementary material). We discarded the cases with more than one dominant peak in molecular gas along the line of sight of the cloud and the cases where the individual cloud contribution to the total ($\text{HI}+\text{H}_2$) gas column density was

$< 20\%$; this condition minimizes the contamination of the cloud’s γ -ray emission by photons produced in the same direction but outside the cloud. This allows the localization of the γ -ray production region on the scale of the cloud dimensions (~ 100 pc). Finally, from the selected list, we had to exclude those clouds located in regions crowded of sources of the 3FGL *Fermi*-LAT catalog [13] or spatially coincident with bright γ -ray source from the H.E.S.S. Galactic Plane Survey (HGPS) [14]. After the application of all these filters, we were left with only 12 clouds.

To the sample, we added three relatively distant clouds, Cepheus, MonOB1 and Maddalena located at distances between 0.8 and 2 kpc. The recently reported distance measurements to these objects [15] revealed promising values of the parameter $A \geq 1$ for the detection of γ -rays.

Finally, we included in the list three nearby clouds, Orion A, Taurus and Lupus, as representatives of the Gould Belt complex. The first two have been already analyzed in previous works e.g. [16, 17]), thus the comparison of the results of our data reduction with these independent studies can be used to cross-check the reliability and consistency of the approaches and approximations invoked in our work. The locations of the above 18 GMCs are shown in Fig.1), and their general properties (coordinates, masses, distances, values of the A parameter) are summarized in Table II. We differentiated the selected objects in six different rings centred at the Galactic Centre. The differentiation is not strict as cloud distances are affected by non-negligible uncertainties. The distance errors are included in the plot, and are reported in Table II. Generally, the distance uncertainty is transferred to the uncertainty in the γ -ray flux estimate. However, in the specific case of molecular clouds, the γ -ray flux is proportional to the A parameter, $A = M_5/d_{\text{kpc}}^2$ which is independent of the distance because $M_5 \propto d_{\text{kpc}}^2$. Therefore the flux estimate is not influenced by the distance uncertainty either.

We analyzed *Fermi*-LAT data accumulated for more than nine years, from MET 239557417 (4th August 2008) to MET 533045411 (22nd November 2017), in the energy band 0.8-800 GeV. The threshold at 0.8 GeV was chosen to take advantage of the better angular resolution, hence to reduce the source confusion. We considered PASS8 data and selected ‘FRONT+BACK’ events (evtype=3). We cut in zenith angles ($z_{\text{max}}=90^\circ$), to avoid the Earth limb events and imposed DATA QUAL==1 && LAT CONFIG==1. The considered ROI was a $10^\circ \times 10^\circ$ square, around the cloud centre. For each molecular cloud, we created a spatial template derived from the CO radio-maps of ref. [11]. For nearby isolated clouds we cut the exact contours of the clouds and integrated the gas over the entire line of sight. For the clouds from ref. [10] we considered the position (l_0, b_0, v_0), the velocity dispersion σ_v and the radius σ_r as given in the

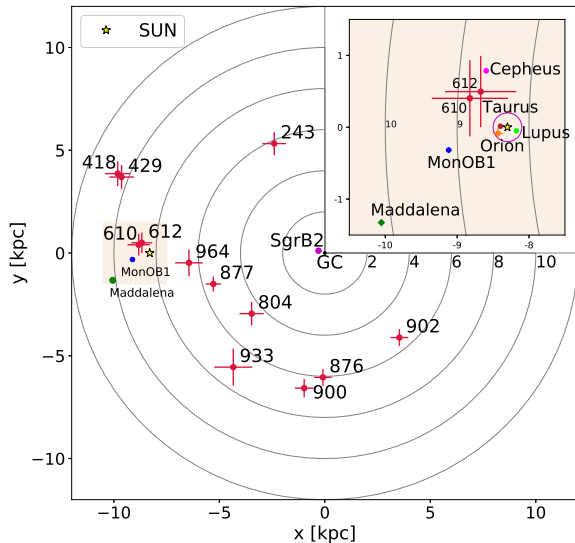


FIG. 1. Positions of the selected GMCs in the Galactic Plane. The reference numbers are from ref. [10]. In the upper right panel is shown a zoomed region surrounding the Sun with the selected nearby clouds. The purple circle, centered on the Sun, represents the approximate position of Gould Belt. The location of the Sgr B2 complex in the Galactic Center is also shown. The positions and their relative uncertainties are taken from refs.[10], [15] and [18].

catalog. As explained in refs. [10] and [19], due to the different gas density profiles, the radius of the CO emitting region σ_r is generally smaller than the radius R of the H_2 region. We assumed $R = \eta \sigma_r$, with $\eta = 1.91$, as calculated in [19]. We considered then a box of side $2R$, and width $\Delta v = 2\sqrt{2 \ln 2} \sigma_v$, integrated over the velocity. For the spectrum, we assumed a power law model. As a template for the background, we could not use the standard galactic background model of the *Fermi*-LAT collaboration [20], since the emission from the molecular clouds is included there as a background. We built then a customized background model, by considering the main channels of production of γ rays above 1 GeV: the π^0 -decay component, the inverse Compton scattering and the extra-galactic diffuse radiation. We created a spatial template of the π^0 -decay emission by considering the gas map of HI [12] and CO [11], from which we excluded the cloud. We assumed a power law spectrum. What concerns the Inverse Compton scattering, we took the output map $^S Y^Z 10^R 30^T 150^C 2$ from `galprop`¹ [21]. For the isotropic extra-galactic component we derived a model

by fitting a 30° region centered in $l, b = (150^\circ, 90^\circ)$, where the Galactic contribution (pion decay and IC) is minimum. As starting model we included the sources from the 3FGL catalog [13]. In the fit we left all the spectral parameters of the diffuse components free, as well as all the sources within 3 degrees from the cloud. The residuals are showed in the supplementary part.

In Fig. 2 we show the Spectral Energy Distributions (SEDs) of all analyzed clouds, the errorbars represent the statistical uncertainty, plots with the systematic uncertainty are reported in the supplementary material. At the bottom of the figure is shown the SED of Sgr B2 complex, as reported in ref. [22], as well as the SEDs of three clouds of the Gould Belt system, Orion A, Taurus and Lupus. The new results, based on 9 years data of *Fermi*-LAT are in good agreement with previous studies of the Gould Belt region [16, 17, 23–25]. The plotted spectral points are normalized to $A=1$ and compared to the γ -ray fluxes expected from interactions of CRs described by the locally measured CR flux (see Eq.1 in the supplementary material). The γ -ray fluxes from GMCs with galactocentric distances more than 8 kpc, including *all* nearby high latitude clouds, are in good agreement with the theoretical predictions made under the assumption that the CR fluxes and energy spectra coincide with the direct CR measurements reported by the AMS collaboration. The same is true for the Sgr B2 complex [22] in the Galactic Center. Moreover, for all clouds, except for one (the cloud #933) located in the ring between 6 and 8 kpc, we find a γ -ray flux similar to the AMS spectrum. On the other hand clouds located in the 4-6 kpc show enhanced γ -ray fluxes and likely harder energy spectra.

From the SEDs of γ rays one can extract direct information about the energy density of the parent CR protons assuming that the inelastic proton-proton and proton-nuclei interactions with production and decay of π^0 -mesons are responsible for the major fraction of the detected γ -rays. For this purpose, we used the `naima` software package [26]. The CR density was fitted as a power law; the spectral indices and the energy densities of CRs above 10 GeV derived for individual clouds are listed in Table I.

To summarize, a robust conclusion can be drawn for *all* clouds with Galactocentric distances larger than 8 kpc, independently of their location in the Galaxy. The results are in good agreement with theoretical predictions assuming that γ rays are produced at interactions of CRs with the gas inside the clouds and that the flux and spectral shape of CRs embedded in the clouds are pretty close to the locally measured CR flux and spectrum as reported by the AMS collaboration [1]. From Fig. 2 we can see good agreement between the observed γ -ray fluxes (normalized for each cloud to the value of the corresponding parameter A) from three regions representing the Gould Belt, the 8-10 kpc ring and the periphery beyond ≥ 10 kpc. While, at first glance, the data relative

¹ <https://galprop.stanford.edu/publications.php?option=supplement&seq=1>

Cloud	$\rho_{0,CR}$ (10 GeV) [10^{-12} GeV $^{-1}$ cm $^{-3}$]	α
418	1.7 ± 0.6	2.78 ± 0.13
429	1.5 ± 0.6	2.7 ± 0.3
Maddalena	2.0 ± 0.7	2.91 ± 0.07
MonOB1	2.4 ± 0.8	3.0 ± 0.1
610	2.0 ± 0.8	3.1 ± 0.3
612	1.4 ± 0.7	2.8 ± 0.4
Cepheus	2.3 ± 0.8	2.88 ± 0.07
Orion A	2.3 ± 0.8	2.83 ± 0.07
Taurus	2.3 ± 0.7	2.90 ± 0.07
Lupus	1.6 ± 0.6	2.69 ± 0.11
933	2.9 ± 1.2	2.81 ± 0.12
900	2.4 ± 0.8	2.88 ± 0.11
964	1.8 ± 0.6	2.73 ± 0.08
876	2.1 ± 0.7	3.01 ± 0.14
243	5.5 ± 1.8	2.93 ± 0.11
877	3.7 ± 1.2	2.75 ± 0.05
902	4.8 ± 1.6	2.99 ± 0.11
804	2.7 ± 0.9	2.67 ± 0.09
Sgr B2 ^a	1.2 ± 0.4	3.1 ± 0.3
AMS-02	1.41	2.85 ^b

^a from [22]

^b Value relative to the rigidity range 45 GV-100 GV as given in[1]

TABLE I. The spectral indices and CR densities at 10 GeV derived from the γ -ray and CO data at the locations of clouds indicated in Fig. 1. Errors on the normalization result from the sum in quadrature of the statistical error deriving from the fit and the 30% uncertainty on the A parameter due to the conversion factor X_{CO}

to the Gould Belt clouds could be interpreted as a result of the dominant contribution by local accelerators to the measured CR flux, the γ -ray data from other clouds, in particular Maddalena, cloud #418 and cloud #429, exclude this scenario. The constancy of the derived densities and the spectral indices of CRs tell us that, most likely, we deal with the sea of CRs. Quite remarkably, the same level of CR density is also derived in the GC region based on the analysis of γ -ray flux below 30 GeV from the Sgr B2 complex in the GC [22] (see Fig.2). To a certain extent, this is an unexpected outcome, given the presence of several potentially powerful accelerators in that region. A plausible explanation of this result could be the effective escape of low-energy CRs from the inner parts of the GC, e.g., due to the fast convection, before they could propagate to large distances and approach Sgr B2.

On the other hand, all four clouds located in the 4-6 kpc ring, show significantly, by a factor of 2-3, enhanced γ -ray fluxes, as well as systematically harder energy spectra compared to γ rays induced by the sea of CRs (see Fig.2). This generally agrees with the results derived from the diffuse γ -radiation of the Galactic Disk [20, 28]. However, one should note that, while the method of derivation of the radial distribution of CRs from the diffuse γ -ray emission is based on a few assumptions and

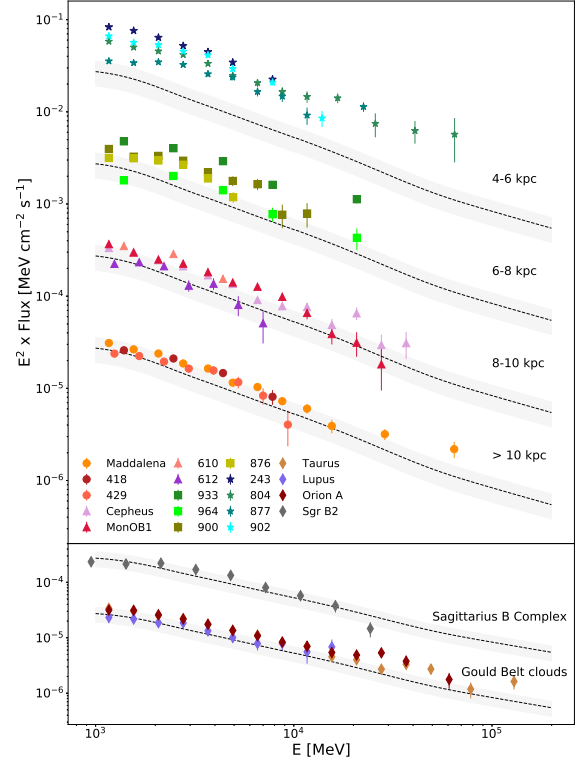


FIG. 2. Spectral Energy Distributions of GMCs. The upper panel: The points are multiplied in order to distinguish them from one another according to their distance from the galactic center, from the bottom to the top: 10-12 kpc (circles); 8-10 kpc (triangles) 6-8 kpc (squares), 4-6 kpc (stars). The SEDs of three Gould Belt clouds and Sgr B2 are shown in the lower panel (below the horizontal line). SEDs are normalized to the parameter of each cloud A (i.e. the derived fluxes are divided to the corresponding values of the A parameter. In some cases the binning at higher energy has been enlarged to include more statistics. The dashed black line indicated for each set of GMCs is the expected SED of a cloud with $A = 1$ calculated for the parent CR proton spectrum reported by the AMS collaboration [1], and using the differential cross-section parametrization from ref. [27]. The parameter that takes into account the contribution of nuclei to the γ -ray production, $\eta = 1.8$, corresponds to the standard compositions of the interstellar gas and CRs. The shaded gray area indicates the 30% uncertainty in M_5/d_{kpc}^2 , due to the CO-to-H $_2$ conversion factor.

gives the *average* density of CRs inside the Galactocentric rings, γ -ray emission from individual clouds provides direct information about the CR density in the localized regions within a few tens of pc. This is an important information which can tell us whether the enhanced γ -ray emission of the 4-6 kpc ring is a result of a global variation of the level of the CR sea on large (kpc) scales or it is caused by an additional component of radiation

on top of the homogeneous sea of CRs. Apparently, any indication of fluctuations both in the flux and the spectral index of γ rays from clouds that belong to the 4-6 kpc ring would give a preference to the second scenario. In particular, a detection of a “nominal” γ -ray flux (i.e. a γ -ray flux expected from the AMS type CR flux) even from a single cloud in the 4-6 kpc ring, would imply that the variations of the CR density in the ring is a result of presence of active or recent accelerators in the proximity of the clouds. The clouds from the 4-6 kpc ring clouds do exhibit variation of γ -ray fluxes but, unfortunately, variations are within the statistical uncertainties (see Fig. 2). On the other hand, the γ -ray flux from the clouds in the 6-8 kpc ring indicates that the CR density should be quite close to the one measured by AMS. Although these cloud enter the “6-8 kpc” zone, their distance to the GC is compatible to 6 kpc within the distance uncertainty, thus they could be part of the “4-6 kpc” ring, especially given that the stellar volume emissivity at 6.5 kpc drops only by a factor of two compared to the maximum at 4.5 kpc [29]. Therefore the “nominal” γ -ray flux implies a minimum, close to the local (AMS) CR density in this part of the ring. What concerns the low level of the CR density, a reason could be the absence of an active CR accelerator nearby.

The above arguments provide a rationale that the radial variations of both the density and energy spectrum of CRs derived from the analysis of diffuse γ -ray emission of the Galactic Disk [20, 28], is not related to the the global CR sea, but has a more local character caused by the large number of cosmic accelerators in the 4-6 kpc ring and correspondingly higher CR density in their neighbourhoods. This seems a direct consequence of the fact that most of the active star forming regions, and therefore, the potential particle accelerators, are located within the 4-6 kpc ring. The scales of regions with enhanced CR density depends on the strength and the age of the accelerator. For SNRs with 10^{51} erg mechanical energy release, the CR density in the surrounding ISM can exceed the level of the CR sea up to 100 pc from the accelerator [30]. In the case of young stellar clusters with an overall mechanical luminosity of stellar winds 10^{38-39} erg/s, the regions with enhanced CRs density can extend well beyond 100 pc [31]. Since both types of accelerators are tightly linked to the star-forming regions, they are often surrounded by GMCs. The presence of dense gaseous regions close to particle accelerators creates favourable conditions for effective production of γ rays [30].

In summary, the results obtained in this study unveil a homogeneous sea of Galactic CRs with a constant density and spectral shape close to the flux of directly measured CRs. A deeper exploration and proof of this interpretation requires significantly larger statistics of γ -ray emitting clouds, in particular a denser coverage of Galactocentric distances. Unfortunately, the lack of projects

for a new γ -ray telescope with significantly improved, compared to the *Fermi*-LAT sensitivity at GeV energies, does not give us much hope, at least for the near future, for a significant increase of the number of clouds resolved in γ rays. The prospects are more promising at higher energies. In particular, the sensitivity of the future Cherenkov Telescope Array (CTA) seem to be sufficient for detection of a few “passive” clouds characterized by the parameter $A \geq 1$ in the energy region between 100 GeV and 1 TeV. Moreover, the detection threshold of clouds by CTA in the regions of the 4-6 kpc ring characterized by enhanced CR density and harder spectra, could be as small as $A \sim 0.1$. This would dramatically increases the number of the potentially detectable clouds providing denser mapping of CRs and extension of studies to energies up to 100 TeV and beyond.

* felix.aharonian@mpi-hd.mpg.de

† peron@mpi-hd.mpg.de

‡ ryang@mpi-hd.mpg.de

§ roberta.zanin@mpi-hd.mpg.de

¶ sabrinacasanova@gmail.com

- [1] M. Aguilar et al. (AMS), Phys. Rev. Lett. **114**, 171103 (2015).
- [2] H. Ahn, P. Allison, M. Bagliesi, J. Beatty, G. Bigongiari, J. Childers, N. Conklin, S. Coutu, M. DuVernois, O. Ganel, et al., The Astrophysical Journal Letters **714**, L89 (2010).
- [3] G. Ambrosi, Q. An, R. Asfandiyarov, P. Azzarello, P. Bernardini, B. Bertucci, M. Cai, J. Chang, D. Chen, H. Chen, et al., Nature **552**, 63 (2017).
- [4] H.E.S.S., “Probing local sources with high energy cosmic ray electron” (2017).
- [5] M. e. a. Aguilar (AMS Collaboration), Phys. Rev. Lett. **114**, 171103 (2015).
- [6] F. A. Aharonian and A. M. Atoyan, A&A **362**, 937 (2000), astro-ph/0009009.
- [7] A. W. Strong, I. V. Moskalenko, and O. Reimer, The Astrophysical Journal **613**, 962 (2004).
- [8] F. Aharonian, Space Science Reviews **99**, 187 (2001).
- [9] S. Casanova, F. A. Aharonian, Y. Fukui, S. Gabici, D. I. Jones, A. Kawamura, T. Onishi, G. Rowell, H. Sano, K. Torii, et al., Publications of the Astronomical Society of Japan **62**, 769 (2010).
- [10] T. S. Rice, A. A. Goodman, E. A. Bergin, C. Beaumont, and T. M. Dame, The Astrophysical Journal **822**, 52 (2016).
- [11] T. M. Dame, D. Hartmann, and P. Thaddeus, The Astrophysical Journal **547**, 792 (2001).
- [12] N. B. Bekhti, L. Flöer, R. Keller, J. Kerp, D. Lenz, B. Winkel, J. Bailin, M. Calabretta, L. Dedes, H. Ford, et al., Astronomy & Astrophysics **594**, A116 (2016).
- [13] F. Acero, M. Ackermann, M. Ajello, and e. Albert, ApJS **218**, 23 (2015), arXiv:1501.02003 [astro-ph.HE].
- [14] A. H. et al., A&A **612**, A1 (2018).
- [15] E. Schlafly, G. Green, D. Finkbeiner, H.-W. Rix, E. Bell, W. Burgett, K. Chambers, P. Draper, K. Hodapp, N. Kaiser, et al., The Astrophysical Journal **786**, 29

- (2014).
- [16] A. Neronov, D. Malyshev, and D. V. Semikoz, *A&A* **606**, A22 (2017), arXiv:1705.02200 [astro-ph.HE].
 - [17] R.-z. Yang, E. de Oña Wilhelmi, and F. Aharonian, *Astronomy & Astrophysics* **566**, A142 (2014).
 - [18] F. Comerón, *Handbook of Star Forming Regions* **2**, 295 (2008).
 - [19] E. Rosolowsky, J. Pineda, J. Kauffmann, and A. Goodman, *The Astrophysical Journal* **679**, 1338 (2008).
 - [20] F. Acero, M. Ackermann, M. Ajello, A. Albert, L. Baldini, J. Ballet, G. Barbiellini, D. Bastieri, R. Bellazzini, E. Bissaldi, et al., *The Astrophysical Journal Supplement Series* **223**, 26 (2016).
 - [21] A. E. Vladimirov, S. W. Digel, G. Jóhannesson, P. F. Michelson, I. V. Moskalenko, P. L. Nolan, E. Orlando, T. A. Porter, and A. W. Strong, *Computer Physics Communications* **182**, 1156 (2011), arXiv:1008.3642 [astro-ph.HE].
 - [22] R.-z. Yang, D. I. Jones, and F. Aharonian, *Astronomy & Astrophysics* **580**, A90 (2015).
 - [23] f. c. Ackermann, *ApJ* **755**, 22 (2012), arXiv:1207.6275 [astro-ph.HE].
 - [24] A. et al. (*Fermi*-LAT collaboration), *ApJ* **756**, 4 (2012), arXiv:1207.0616 [astro-ph.HE].
 - [25] A. Neronov, D. V. Semikoz, and A. M. Taylor, *Physical Review Letters* **108**, 051105 (2012), arXiv:1112.5541 [astro-ph.HE].
 - [26] V. Zabalza, *Proc. of International Cosmic Ray Conference 2015*, 922 (2015), 1509.03319.
 - [27] E. Kafexhiu, F. Aharonian, A. M. Taylor, and G. S. Vila, *ArXiv e-prints* (2014), arXiv:1406.7369 [astro-ph.HE].
 - [28] R. Yang, F. Aharonian, and C. Evoli, *Phys. Rev. D* **93**, 123007 (2016), arXiv:1602.04710 [astro-ph.HE].
 - [29] C. C. Popescu, R. Yang, R. J. Tuffs, G. Natale, M. Rushton, and F. Aharonian, *MNRAS* **470**, 2539 (2017), arXiv:1705.06652.
 - [30] F. A. Aharonian and A. M. Atayan, *A&A* **309**, 917 (1996).
 - [31] F. Aharonian, R. Yang, and E. d. O. Wilhelmi, (2018), arXiv:1804.02331 [astro-ph.HE].
 - [32] A. D. Bolatto, M. Wolfire, and A. K. Leroy, *Annual Review of Astronomy and Astrophysics* **51**, 207 (2013).
 - [33] M. Ackermann, M. Ajello, A. Allafort, L. Baldini, J. Ballet, G. Barbiellini, D. Bastieri, K. Bechtol, R. Bellazzini, B. Berenji, et al., *The Astrophysical Journal* **755**, 22 (2012).
 - [34] S. Gabici, F. A. Aharonian, and P. Blasi, *Ap&SS* **309**, 365 (2007), arXiv:astro-ph/0610032.

SUPPLEMENTARY MATERIALS

CLOUD SELECTION

Cloud	l (deg)	b (deg)	Mass ($10^5 M_\odot$)	d (kpc)	R_{GC} (kpc)	A
243	42.04	-0.36	30.3	7.95 ± 0.6	5.85	0.47
418	111.45	0.79	7.9	4.15 ± 0.6	10.58	0.46
429	109.84	-0.29	10.3	3.93 ± 0.6	10.35	0.67
610	142.40	1.38	0.26	0.66 ± 0.55	8.9	0.61
612	126.87	-0.66	0.32	0.62 ± 0.5	8.72	0.83
804	328.58	0.4	24.0	5.66 ± 0.6	4.58	0.75
876	323.61	0.22	60.13	10.2 ± 0.4	6.05	0.58
877	333.46	-0.31	12.6	3.37 ± 0.4	5.53	1.11
900	318.07	-0.21	46.6	9.84 ± 0.4	6.65	0.48
902	340.84	-0.30	115.1	12.53 ± 0.4	5.40	0.73
933	305.49	0.11	29.5	6.82 ± 0.9	7.07	0.63
964	345.57	0.79	2.8	1.92 ± 0.6	6.45	0.75
Taurus	171.6	-15.8	0.06	0.10 ± 0.03	8.40	5.5
Lupus	338.9	16.5	0.01	0.14 ± 0.02	8.17	0.58
Orion A	209.1	-19.9	0.4	0.48 ± 0.07	8.43	1.8
Cepheus	110.7	12.6	1.3	0.86 ± 0.03	8.63	1.76
MonOB1	202.1	1.0	0.9	0.88 ± 0.04	9.12	1.2
Maddalena	216.5	-2.5	8.7	2.22 ± 0.05	10.14	1.8

TABLE II. Parameters of GMCs: Galactic coordinates (l,b), masses M , distances from the Earth d , Galactocentric distances R_{GC} , and the A parameter. The information about the distant GMCs (the upper part of the table) are from ref.[10], about nearby clouds (lower part of the table, below the horizontal line) are from [15], except for Lupus which is taken from from [18].

The complete sample of Giant Molecular Clouds (GMCs) analyzed in this work is reported in Table II. We analyzed 18 MCs from different locations. 12 clouds were selected from the recent catalog of Rice et al. [10], that contains 1064 objects in the four quadrants of the Galaxy. Despite the large number of MCs included in this catalog, the number of good candidates for *Fermi*-LAT had to be reduced to 12. The selection was made based on i) the A parameter, i.e. the expected γ -ray flux; ii) the distribution of the gas on the line of sight iii) vicinity to known gamma-ray sources. Below we explain in details how we applied these criteria. We then considered the clouds listed in ref. [15] as they provide a new improved estimation of the distance of these objects. Among them we chose to reanalyze 3 clouds of the Gould Belt, as they are representative of the local (~ 200 pc) environment, and cross-checked our methods with former results [16, 17]. We included in the analysis Lupus, that was not studied before, and we performed a new analysis on Taurus and Orion A, by taking advantage of the new improved statistics. From the same list we picked three other objects that stands outside the Gould Belt system, at a distance from 0.8 kpc to more than 2 kpc, since they have a high enough parameter A ($\equiv M_5/d_{kpc}^2$) to be studied.

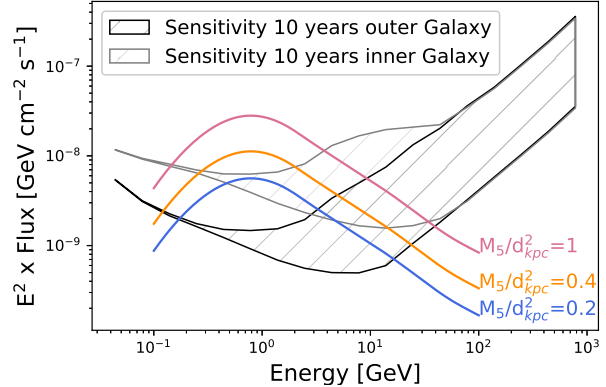


FIG. 3. Comparison between the *Fermi*-LAT sensitivity at different sky coordinates and the flux of MCs with different M_5/d_{kpc}^2 . The gray lines are relative to inner Galaxy, and is delimited by the point-like sensitivity curve and the 1° sensitivity, calculated as explained in the text. Black lines refer instead to the outer and high latitude region of the Galaxy.

Expected emission vs. sensitivity

We compared the γ -ray flux expected from a MC with the sensitivity of *Fermi*-LAT (10 years). We calculated the expected gamma-ray flux from an ideal molecular cloud as:

$$F_\gamma(E_\gamma) = 1.25 \times 10^{19} A \xi_N \int dE_p \frac{d\sigma}{dE_\gamma} F_p(E_p) \quad (1)$$

by assuming a nuclear enhancement factor $\xi_N=1.8$ and a differential cross section as given in [27]; a parent spectrum $F_p(E_p)$ as measured by the AMS02 experiment [1], and different values for the parameter A , ranging from 0.2 to 1.

We compared this flux with the sensitivity of *Fermi*-LAT, multiplied by a factor $\sqrt{\sigma_{PSF}^2 + R^2}/\sigma_{PSF}$, that accounts for the worsening in sensitivity due to the source extension, R . In figure 3 the 10 years sensitivities for the inner and the outer Galaxy are shown; the shadowed area illustrates the point-like sensitivity and the sensitivity calculated for a 1-degree source. This shows that *Fermi*-LAT is capable to detect MCs with $A \gtrsim 0.4$, when smaller than $\sim 1^\circ$.

Gas abundance on the line of sight

Differently from its atomic counterpart, molecular hydrogen (H_2) is not uniformly spread in the Galactic Disk, it rather tends to concentrate in small regions. The majority of the Galactic H_2 is embedded in MCs, where the environment is cold enough ($T \sim 10$ -20 K) to allow the presence of matter in form of molecules. MCs are then special regions where the gas distribution peaks. Measuring the flux in the direction of a molecular cloud allows

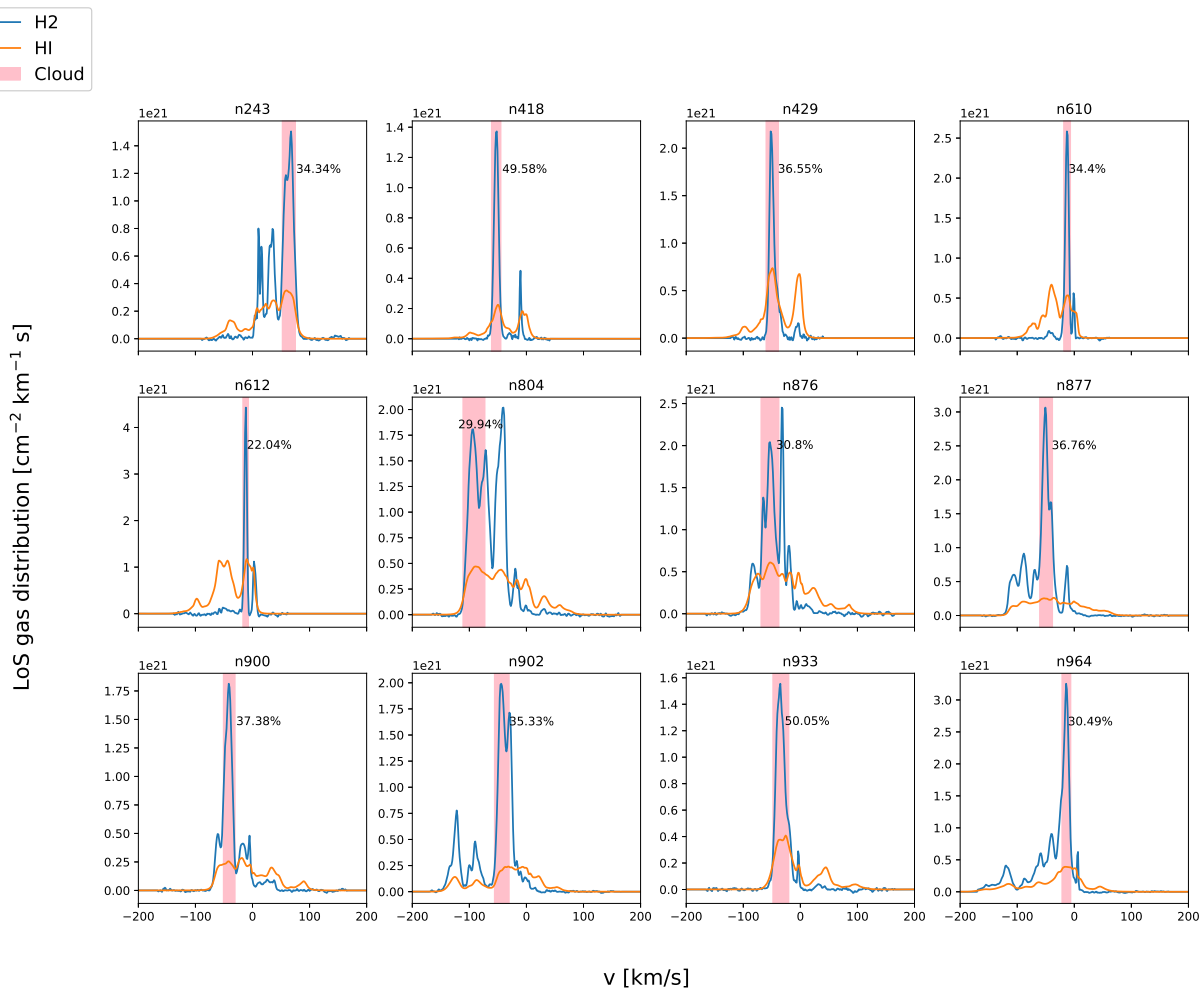


FIG. 4. Gas distribution along the line of sight in the regions of the analyzed MCs. The pink area delimits the velocity-range of the cloud. Blue lines represent the distribution of molecular hydrogen, and orange lines the atomic one. The conversion factors here were $X_{CO} = 2 \times 10^{20}$ and $X_{HI} = 1.8 \times 10^{18}$.

us to localize the origin of this emission in few tens of parsecs. To allow a precise localization and limit the uncertainties due to fore- and background gas we selected clouds that were the dominant objects in terms of gas column density, both of H_2 and of HI, along the line of sight (L.o.S.).

H_2 produces no detectable emission in such cold environment, since it has no permanent dipole momentum. Its distribution has to be traced by other molecules. We chose to consider the Carbon Monoxide (CO), that has a clear emission in the radio waveband at 115 GHz. Here we considered the data from the jointed surveys taken with the CfA 1.2 m telescope and other similar instruments in Cerro Tololo [11]. They provide the data-cubes (Galactic Longitude (l), Galactic Latitude (b) and Radial Velocity (v)) of the brightness temperature, T_b , of the CO. This quantity is related to the H_2 column den-

sity by:

$$n(l, b) [cm^{-2}] = X_{CO} \int dv T_b(l, b, v) [km s^{-1} K] \quad (2)$$

that depends on the CO-to- H_2 conversion factor, X_{CO} . We set $X_{CO} = 2 \times 10^{20} cm^{-2} K^{-1} km^{-1} s$ according to [32].

Atomic hydrogen is considered only as background gas in the analysis and not as signal, since it is hard to isolate the HI in the cloud from the rest of the column density. We considered the data-cube from the HI4PI collaboration[12], that maps the 21-cm emission line of the neutral hydrogen. Analogously to the molecular gas density, the HI density is directly proportional to the brightness temperature of the 21-cm line, with here a conversion factor given in ref. [12] of $X_{HI} = 1.83 \times 10^{18} cm^{-2} K^{-1} km^{-1} s$. It is worth to stress that this conversion factor is derived with the assumption of optically thin emission. We are aware that this could re-

sult in a *underestimation* of the background that could consequently result in a *overestimation* of the cloud flux (more details in the discussion of the background evaluation). This strengthens the importance of choosing clouds whose density overcomes the HI density.

In figure 4 we show the derived H_2 and HI distribution by integrating $T_b(l, b, v)$ in the regions that define the clouds spatial extent, i.e. in a square of $2R$ side², centered at the cloud coordinates. The pink area represents the cloud extension in the L.o.S. The velocity range has been calculated from the velocity dispersion, σ_v given in the catalog [10], as $\Delta v = \sqrt{2 \ln 2} \sigma_v$, approximating the cloud profile to a Gaussian.

The relative contribution to the gas L.o.S. of the chosen sample of clouds is reported in III.

Cloud	$\frac{n_H(\text{cloud})}{n_H(H_2)}\%$	$\frac{n_H(\text{cloud})}{n_H(H_2+HI)}\%$
243	52.63	34.34
418	82.67	49.58
429	85.72	36.55
610	82.35	34.4
612	73.42	22.04
804	44.57	29.94
876	53.24	30.8
877	49.17	36.76
900	58.34	37.38
902	47.12	35.33
933	83.51	50.05
964	41.28	30.49

TABLE III. Percentage contribution of the clouds to the relative column of gas. Ratio are calculated over molecular gas, and total (H_2+HI) gas.

MCs chosen for the analysis are the dominant object in terms of molecular gas and have a ratio $n_H(\text{cloud})/n_H(H_2 + HI)$ of at least 20%. This reduces the confusion that could raise when having other smaller clouds in the back- or fore-ground, and therefore allows to identify the origin of the measured photons with the cloud itself.

γ ray sources in the vicinity

We considered the 3FGL [13] and the HGPS [14] catalogs of γ -ray sources and studied the known sources located in the vicinity of our sampled clouds. We discarded the clouds that have many overlapping sources (e.g clouds 151, 190, 842) and the clouds that are in the proximity of strong H.E.S.S. sources (e.g. 269, 292, 897). The 12 selected clouds have no know sources on top of

them, but some of them have some confuse or unidentified source overlapping. Specifically clouds 610, 902, 933 have a faint confused source on top of them that results negligible ($TS < 10$) after the fit. Cloud 804, 877 and 964 have significant ($TS > 25$) sources that can not be eliminated. We tested the influence of those on the cloud SEDs by fitting the model with and without these sources. From the comparison we can conclude that the spectral shape is not influenced, while the normalization changes of $\lesssim 20\%$, so by a factor smaller than the systematic uncertainty.

THE FERMI-LAT ANALYSIS

The essential steps of the analysis are described in the main text how we calculated systematic uncertainties.

Systematic uncertainties

We considered the following sources of systematic errors:

New sources. At the moment of writing the 4FGL catalog has not been publicly released, so we made use of the 3FGL catalog of gamma ray sources. The 3FGL catalog is based on 4 years of data, so we expect to reveal several new sources. We identified as new sources in our ROI any residual with a significance larger than 5σ ($TS > 25$), we then included them in the background model and re-fitted the data until there were no more significant spots (see fig 9). In few cases some sources appeared at the edges of our analyzed clouds. Thus we evaluated the effect of this sources on our resulting spectral points by subtracting the SED obtained before including these sources and after the inclusion. The difference from the two sets of spectral points is estimated to be at worst $\sim 20\%$ for what concerns the normalization and does not affect the slope. This uncertainty is included in the systematic errors for each cloud.

Radial dependent CR distribution. Studies of the diffuse γ -ray emission showed that the cosmic ray spectra have different shapes at different distances from the GC. In particular refs. [20, 28] show that the CR density increases and spectrum hardens towards the inner Galaxy. In our analysis we assumed the CR radial distribution to be uniform in the considered ROI. To test the possible deviation we derived the γ -ray spectra assuming a background derived using the radial dependent CR distribution. Following ref.[28], we divided the gas in 6 galactocentric rings and assigned to each of them the corresponding normalization and spectral index of CRs derived in their work. The difference between the two SEDs is of the order of 10% in terms of normalization and it is summed in quadrature to the other systematic uncertainties.

² R here is the radius of the hydrogen region, that is proportional to the radius of the CO emitting region by a factor $\eta = 1.91$, as explained in the main text and in ref. [19]

Optically thin HI. It can occur, especially at low latitudes, that the 21-cm emission is self shielded by layers of colder gas that stands along the L.o.S. The data from the HI4PI collaboration are not corrected for this self absorption effect, meaning that they have to be considered as a lower limit approximation, and the derived HI column density has to be taken as a lower limit. The corrected value for N_{HI} is given as:

$$N_{HI} = -1.823 \times 10^{18} T_s \int dv \ln \left[1 - \frac{T_B(v)}{T_s - T_0} \right] \quad (3)$$

as explained in [33]. HI in this work enters as background component and we are aware that an underestimation of the background could lead to overestimate our spectral points. We tested the influence of this approximation by performing an independent analysis on the same data, correcting N_{HI} according to eq. 3, with $T_s = 150$ K and $T_0 = 2.66$ K as assumed by the *Fermi*-LAT collaboration [33]. Even though the selected clouds are all dominant in terms of column density over the HI background the resulting spectrum seems to be affected by the choice of the HI background by a factor that could vary from 20 to 50 %. The difference between the two spectral sets has been included as systematic error.

Different gas tracer. Interstellar dust should be a more comprehensive tracer of the gas distribution, since in principle it is sensitive also to the fraction of gas for which we don't have a direct radio detection (due to self absorption or saturation). However, dust opacity maps are bi-dimensional, and hence are not suitable to trace distant non-isolated objects. We used the Planck dust opacity map as spatial template to analyze six nearby clouds (Orion A, Taurus, Lupus, Cepheus, Monoceros OB1 and Maddalena). We checked in the CO data that these objects were isolated on the line of sight. The difference between the two analysis is included in the systematic uncertainty for these sources, and amounts on average to 30-50 %.

All the contribution were then summed in quadrature to obtain the final systematic uncertainty, differentiating between lower errors and upper errors.

Counts profile

In order to check the results of our fit we compared the integrated profile of counts with the model resulting after the fit, see Fig. 5. The profile were obtained by selecting a slice in DEC corresponding to the spatial extension of the clouds and integrating over the declination. In the plot we show the fitted total model, together with the model of the cloud, the background gas and the sum of the two. We can see that the total model well represents the observed counts and that the pion decay emission of the gas is, as expected, provides the dominant contribution to the observed emission.

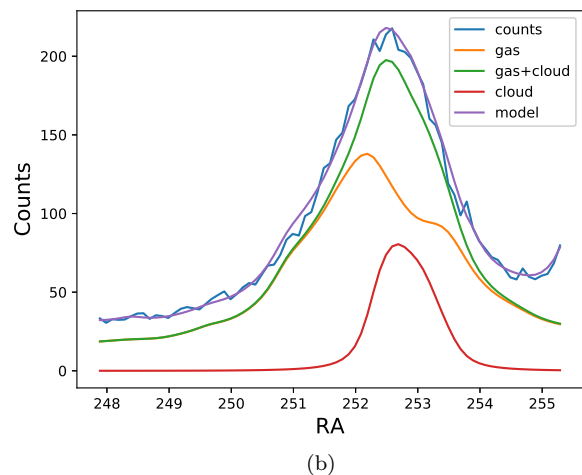
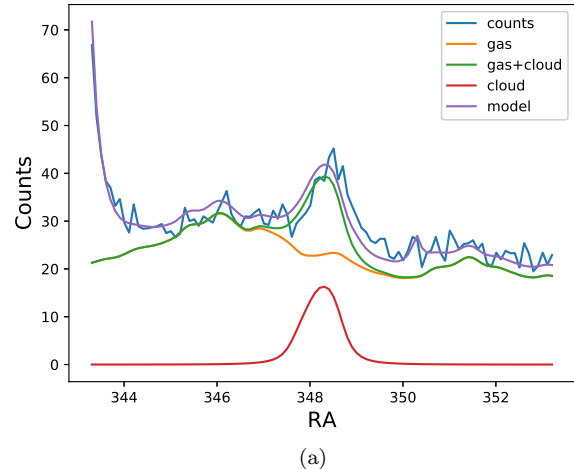


FIG. 5. Comparison between the data counts and the model counts of the cloud and of the background gas, derived after the fit, from a slice in DEC correspondent to the extension of the cloud. We show two examples: in (a) cloud 418 that is in the outer Galaxy, in (b) cloud 902 located in the inner Galaxy.

1

RESULTS

The resulting γ -ray spectra with the relative systematic errors are shown in Fig. 6, in the main text, and are compared with the theoretical flux, calculated as explained in the following. All the points plotted have $TS > 5$. These SEDs were derived after subtraction of all significant sources, the residual maps are shown in figure 8. From these points we derived the proton density with *naima*[26] and we compared it with the one measured by the AMS experiment [1].

Expected gamma-ray flux

The resulting γ -ray SEDs are shown in Fig. 6, where they are compared with a theoretical curve. The expected curve is calculated as in eq.1, by assuming a parent proton spectrum as the one measured by AMS02 [1], $\xi_N = 1.8$ and the cross section as in [27]. The theoretical flux is proportional to the parameter A , that is affected by an uncertainty of 30%, entirely due to uncertainty on the conversion factor X_{CO} . This uncertainty consequently is reflected to the normalization of the curve. In the plot this uncertainty is represented by the shaded gray areas.

Following Rosolowsky [19], the mass and consequently the parameter $A=M_5/d_{kpc}^2$ is computed starting from the CO emission. Basically one needs to convert the CO luminosity in H column density $n(l, b)$ through the renowned conversion factor X_{CO} , calculate the total column density within the cloud, and from that recover the mass. In practice one computes:

$$M = 2m_p X_{CO} \sum_{i,j} W_{ij}(l_i, b_i) \Delta l \Delta b \left(\frac{\pi}{180} \right)^2 d^2$$

where $W_{ij}(l_i, b_i) \equiv \int_{v_{min}}^{v_{max}} T_{CO}(l, b, v) dv$ is the integrated brightness temperature of CO. We can notice that the mass is directly related to the distance d^2 , since it determines the physical extension from the observed angular one. On the other hand, this allows to have an estimation of the M_5/d_{kpc}^2 factor directly from the CO data, that is independent of the uncertainties of mass and distance, in fact it can be expressed as:

$$\frac{M_5}{d_{kpc}^2} \approx 32 \sum_{i,j} W_{ij}(l_i, b_i) \Delta l \Delta b \left(\frac{\pi}{180} \right)^2$$

The dominant uncertainties here is in the X_{CO} , that is considered to be of 30% as suggested by Bolatto [32].

Helium fraction of the ISM here is not taken into account, differently from what is done in [10] where they include it as a further factor 1.36. Helium contribution in γ -ray emission from pp interaction is already accounted in the nuclear enhancement factor, that we assumed to be 1.8, according to [27].

Proton density and relative uncertainties

The differential γ -ray flux, calculated in Eq. 1 can be expressed as function of the CR density, by recalling that $\rho_{CR} = \frac{4\pi}{c} J(E_p)$, where $J(E_p)$ is the CR-proton spectrum:

$$F_\gamma(E_\gamma) \propto \frac{M_5}{d_{kpc}^2} \int dE_p \frac{d\sigma}{dE_\gamma} \frac{4\pi}{c} \rho_{CR} \quad (4)$$

To estimate ρ_{CR} we made use of `naima` [26]. In MCs, the gas density is high, so the main γ -ray production mechanism of γ rays is the decay of neutral pions produced in the collision of CR nuclei with the ambient gas [34]. We assume the pion-emission to be the only production channel for the observed radiation.

`naima` uses a modified version of Eq. 4, namely:

$$\begin{aligned} F_\gamma(E_\gamma) &= \frac{\langle n_H \rangle}{d^2} \int dE_p \frac{d\sigma}{dE_\gamma} \int_V dV \frac{4\pi}{c} \frac{dN_p}{dE dV} \\ &= \frac{\langle n_H \rangle}{d^2} \int dE_p \frac{d\sigma}{dE_\gamma} \frac{4\pi}{c} \frac{dN_p}{dE} \end{aligned}$$

Our γ -ray data start from ~ 1 GeV and therefore they are tracing CRs of energies $\gtrsim 10$ GeV. For this reason we assumed the initial form of the CR distribution to be a power law ($dN_p/dE = F_0(E/E_0)^{-\alpha}$), and we estimated the parameter F_0 , and α . We initially set $\langle n_H \rangle = 1 \text{ cm}^{-3}$ and $d_{kpc} = 1$, so that the output normalization is $F'_0 = \frac{\langle n_H \rangle}{d_{kpc}^2} F_0$. This allows to write the CR density normalization, $\rho_{0,CR}$, in terms of A and known quantity only, by recalling that $\rho_{CR} = \frac{1}{V} \frac{dN_p}{dE_p}$:

$$\rho_{0,CR} = \frac{F_0}{V} = \frac{d_{kpc}^2}{\langle n_H \rangle V} F'_0 = \frac{d_{kpc}^2}{10^5 \frac{M_\odot}{m_p} M_5} F'_0$$

In this way the systematic error in the esteem of F_0 is reduced to only the uncertainty on $A = M_5/d_{kpc}^2$, that comes from the conversion factor X_{CO} , as discussed above. The resulting parameters are reported in Table I, in the main text. In figure 6, the derived parameter with the relative uncertainty for all the clouds are plotted as a function of their galactocentric distance, R_{gal} .

In Fig. 7 we compare the CR density as derived by the fitting, with the AMS02 local density. The shaded reddish bands include the combination of the statistical error and the systematic 30% uncertainty on the normalization $\rho_{0,CR}$; we didn't include the error on the slope.

* felix.aharonian@mpi-hd.mpg.de

† peron@mpi-hd.mpg.de

‡ ryang@mpi-hd.mpg.de

§ roberta.zanin@mpi-hd.mpg.de

¶ sabrinacasanova@gmail.com

- [1] M. Aguilar et al. (AMS), Phys. Rev. Lett. **114**, 171103 (2015).
- [2] H. Ahn, P. Allison, M. Bagliesi, J. Beatty, G. Bigongiari, J. Childers, N. Conklin, S. Coutu, M. DuVernois, O. Ganel, et al., The Astrophysical Journal Letters **714**, L89 (2010).
- [3] G. Ambrosi, Q. An, R. Asfandiyarov, P. Azzarello, P. Bernardini, B. Bertucci, M. Cai, J. Chang, D. Chen, H. Chen, et al., Nature **552**, 63 (2017).

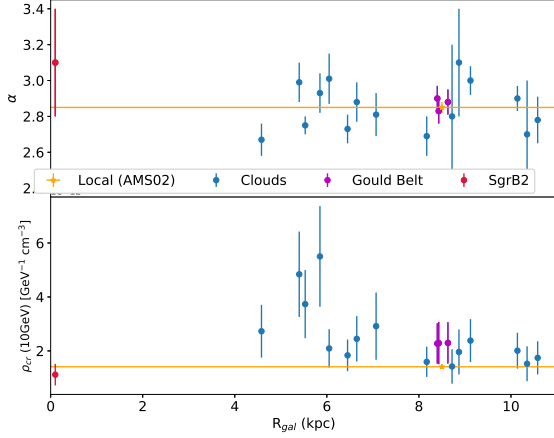


FIG. 6. Cosmic Ray density parameters plotted against the galactocentric distance of the clouds: normalization $\rho_{0,CR}$ evaluated at 10 GeV, and slope α . The values for SgrB2 are taken from [22].

- [4] H.E.S.S., “Probing local sources with high energy cosmic ray (2017).
- [5] M. e. a. Aguilar (AMS Collaboration), Phys. Rev. Lett. **114**, 171103 (2015).
- [6] F. A. Aharonian and A. M. Atoyan, A&A **362**, 937 (2000), astro-ph/0009009.
- [7] A. W. Strong, I. V. Moskalenko, and O. Reimer, The Astrophysical Journal **613**, 962 (2004).
- [8] F. Aharonian, Space Science Reviews **99**, 187 (2001).
- [9] S. Casanova, F. A. Aharonian, Y. Fukui, S. Gabici, D. I. Jones, A. Kawamura, T. Onishi, G. Rowell, H. Sano, K. Torii, et al., Publications of the Astronomical Society of Japan **62**, 769 (2010).
- [10] T. S. Rice, A. A. Goodman, E. A. Bergin, C. Beaumont, and T. M. Dame, The Astrophysical Journal **822**, 52 (2016).
- [11] T. M. Dame, D. Hartmann, and P. Thaddeus, The Astrophysical Journal **547**, 792 (2001).
- [12] N. B. Bekhti, L. Flöer, R. Keller, J. Kerp, D. Lenz, B. Winkel, J. Bailin, M. Calabretta, L. Dedes, H. Ford, et al., Astronomy & Astrophysics **594**, A116 (2016).
- [13] F. Acero, M. Ackermann, M. Ajello, and e. Albert, ApJS **218**, 23 (2015), arXiv:1501.02003 [astro-ph.HE].
- [14] A. H. et al., A&A **612**, A1 (2018).
- [15] E. Schlafly, G. Green, D. Finkbeiner, H.-W. Rix, E. Bell, W. Burgett, K. Chambers, P. Draper, K. Hodapp, N. Kaiser, et al., The Astrophysical Journal **786**, 29 (2014).
- [16] A. Neronov, D. Malyshev, and D. V. Semikoz, A&A **606**, A22 (2017), arXiv:1705.02200 [astro-ph.HE].
- [17] R.-z. Yang, E. de Oña Wilhelmi, and F. Aharonian, Astronomy & Astrophysics **566**, A142 (2014).
- [18] F. Comerón, Handbook of Star Forming Regions **2**, 295 (2008).
- [19] E. Rosolowsky, J. Pineda, J. Kauffmann, and A. Goodman, The Astrophysical Journal **679**, 1338 (2008).
- [20] F. Acero, M. Ackermann, M. Ajello, A. Albert, L. Baldini, J. Ballet, G. Barbiellini, D. Bastieri, R. Bellazzini,

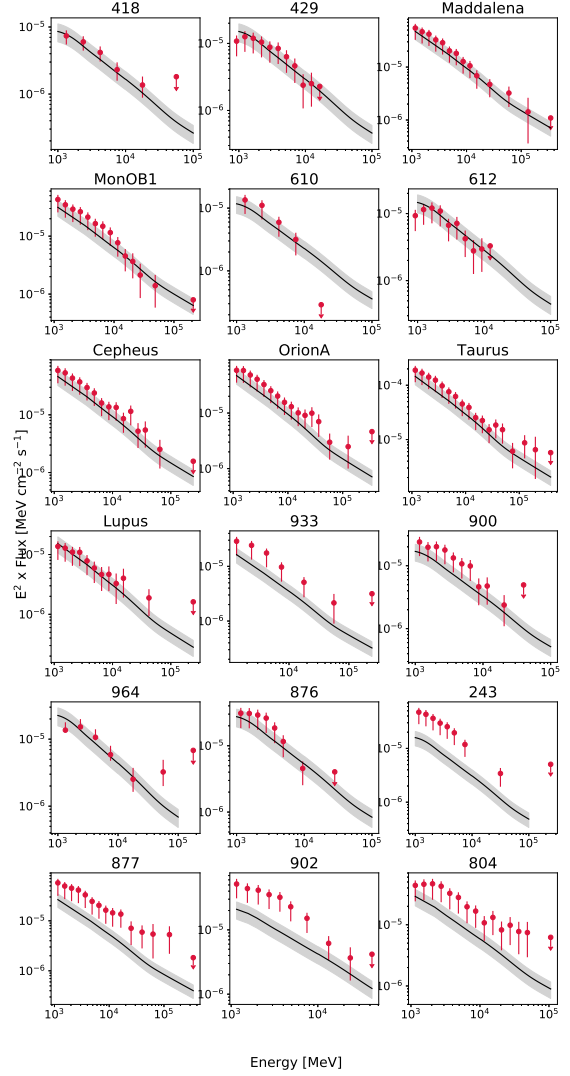


FIG. 7. All the SED (red points) derived in this work, compared with the theoretical flux (black line) calculated as in 1. The shaded gray area represents the 30% uncertainty on the normalization due to the CO to H₂ conversion factor. The order of the figures goes from the most distant cloud of our sample to the closest one to the GC

- E. Bissaldi, et al., The Astrophysical Journal Supplement Series **223**, 26 (2016).
- [21] A. E. Vladimirov, S. W. Digel, G. Jóhannesson, P. F. Michelson, I. V. Moskalenko, P. L. Nolan, E. Orlando, T. A. Porter, and A. W. Strong, Computer Physics Communications **182**, 1156 (2011),

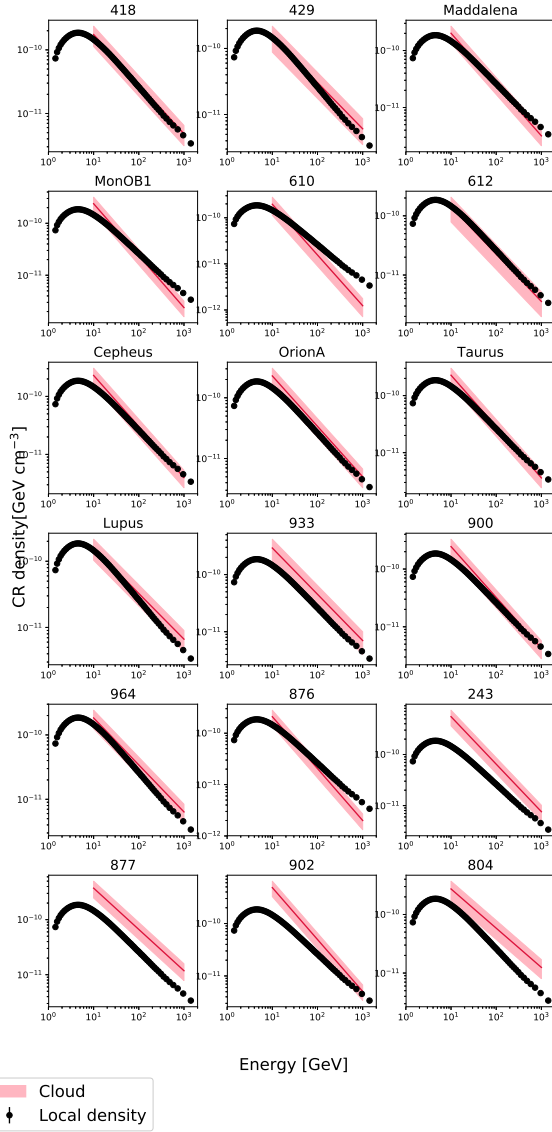


FIG. 8. Derived cosmic ray density for all analyzed clouds, compared with AMS02 measured values. Clouds are ordered from the most distant to the closest ones to the GC.

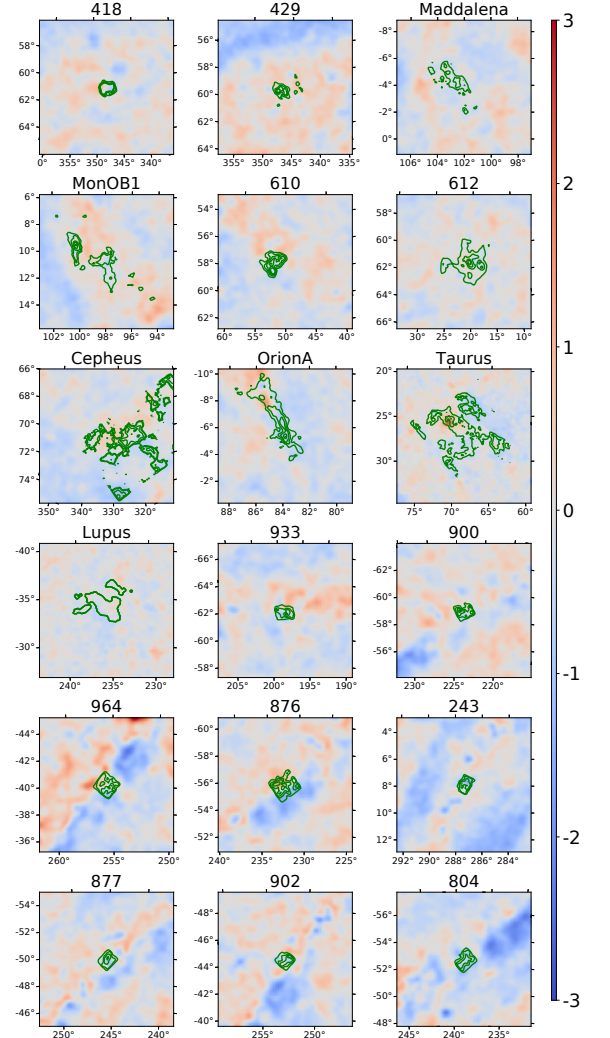


FIG. 9. Residuals maps for all clouds analysed in this work.

- arXiv:1008.3642 [astro-ph.HE].
- [22] R.-z. Yang, D. I. Jones, and F. Aharonian, *Astronomy & Astrophysics* **580**, A90 (2015).
- [23] f. c. Ackermann, *ApJ* **755**, 22 (2012), arXiv:1207.6275 [astro-ph.HE].
- [24] A. et al. (*Fermi*-LAT collaboration), *ApJ* **756**, 4 (2012), arXiv:1207.0616 [astro-ph.HE].
- [25] A. Neronov, D. V. Semikoz, and A. M. Taylor, *Physical Review Letters* **108**, 051105 (2012), arXiv:1112.5541 [astro-ph.HE].
- [26] V. Zabalza, Proc. of International Cosmic Ray Confer-

- ence 2015 , 922 (2015), 1509.03319.
- [27] E. Kafexhiu, F. Aharonian, A. M. Taylor, and G. S. Vila, ArXiv e-prints (2014), arXiv:1406.7369 [astro-ph.HE].
- [28] R. Yang, F. Aharonian, and C. Evoli, *Phys. Rev. D* **93**, 123007 (2016), arXiv:1602.04710 [astro-ph.HE].
- [29] C. C. Popescu, R. Yang, R. J. Tuffs, G. Natale, M. Rushton, and F. Aharonian, *MNRAS* **470**, 2539 (2017), arXiv:1705.06652.
- [30] F. A. Aharonian and A. M. Atoyan, *A&A* **309**, 917 (1996).
- [31] F. Aharonian, R. Yang, and E. d. O. Wilhelmi, (2018),

- arXiv:1804.02331 [astro-ph.HE].
- [32] A. D. Bolatto, M. Wolfire, and A. K. Leroy, *Annual Review of Astronomy and Astrophysics* **51**, 207 (2013).
- [33] M. Ackermann, M. Ajello, A. Allafort, L. Baldini, J. Ballet, G. Barbiellini, D. Bastieri, K. Bechtol, R. Bellazzini, B. Berenji, et al., *The Astrophysical Journal* **755**, 22 (2012).
- [34] S. Gabici, F. A. Aharonian, and P. Blasi, *Ap&SS* **309**, 365 (2007), arXiv:astro-ph/0610032.